On the Orderly Nature of the Motion of Nonspherical Aerosol Particles

II. Inertial Collision between a Spherical Large Droplet and an Axially Symmetrical Elongated Particle

ISAIAH GALLILY[1,2] AND AARON-HI COHEN

Department of Atmospheric Sciences, the Hebrew University of Jerusalem, Jerusalem, Israel

Received May 17, 1978; accepted August 9, 1978

The efficiency of inertial collision between prolate ellipsoidal particles and a spherical large droplet was calculated. The calculation was performed by simultaneously solving both the equation of translation and the equation of rotation of the spheroids for various initial orientations of the latter. The field of flow around the large droplet was acquired from a previous numerical solution of the Navier–Stokes equation, and the expression for the fluid dynamic torque was taken from Jeffery [*Proc. Roy. Soc.* **102A**, 161–179 (1923)]. The results show a pronounced sensitivity to the initial conditions of orientation. If compared to the collisional efficiencies of a volumetrically equivalent sphere, the efficiencies of the ellipsoidal elongated particles in the investigated cases are up to about 3.5 times greater than the former. The calculational method is applicable to the inertial impaction of any aerosol particle of a general ellipsoid shape which may simulate straight fibers, needles, or oblate (atmospheric) particles of mineral origin.

I. INTRODUCTION

Background

Mutual collisions between aerosol particles as well as collisions between particles and larger bodies are a common occurrence in nature, industry, and laboratory where dust scavenging by falling rain drops, pollution abatement, and coagulation are but a few examples.

Dealing with particle collisions, it is convenient to distinguish between collisional processes such as inertial impaction which can be treated deterministically and processes such as diffusion which are best considered as a stochastic chain of events. Usually, depending on the ratio between the orderly kinetic and the thermal energy of the particle, it is only one type of a process which predominates. In all processes, however, it is necessary to pay attention to the shape of the particles composing the aerosol system. The latter can be classified into that consisting of spherical, nonspherical, or both kinds of particles. The two kinds of particles are significantly different from each other because of their symmetry properties. Thus, compared with the motion of spherical aerosol particles, that of the nonspherical ones is a much more complex phenomenon often characterized by a drift, an aerodynamic coupling between translation and rotation, and, sometimes, wobbling, all of which are not encountered in the spherical case.

Inertial impaction of aerosol particles on an obstacle is due to the deviation of the former from their original flow lines on account of their inertia (Fig. 1). The general motion of an *arbitrary particle* in this

[1] On sabbatical leave at the Department of Atmospheric Sciences, University of California, Los Angeles.

[2] To whom correspondence should be directed.

0021-9797/79/020338-19$02.00/0

process is given by the equation of translation[3]

$$m d\mathbf{v}_M/dt = \sum_i \mathbf{F}_{e,i} + \mathbf{F}_F \qquad [1]$$

and rotation

$$d(\mathbf{I}_M \cdot \boldsymbol{\omega})/dt = \sum_i \mathbf{T}_{M,e,i} + \mathbf{T}_{M,F}. \qquad [2]$$

The critical terms in Eqs. [1] and [2] are $\mathbf{F}_F$ and $\mathbf{T}_{M,F}$ which can be formally expressed for an isolated particle that steadily moves through a continuous fluid ($K_n \ll 1$) in a creeping motion ($R_e^t, R_e^r \ll 1$), in terms of a particle's intrinsic and symmetric second-rank tensors of translation, $\mathbf{K}$, rotation, $\boldsymbol{\Omega}_R$, and coupling, $\mathbf{C}_R$(1).

For ellipsoidal particles carried in an arbitrary flow $\mathbf{u}$ at the above mentioned conditions, the $\mathbf{C}_R$ tensor which couples particle translation and rotation to produce a resistance $\mathbf{F}_F$ and torque $\mathbf{T}_{M,F'}$ is zero. The translational resistance then becomes (2)

[3] For notations see Nomenclature.

$$\mathbf{F}_F = \mu\mathbf{K}\cdot\left[\mathbf{u}_M + \frac{1}{3!}(D^2\mathbf{u})_M + \frac{1}{5!}(D^4\mathbf{u})_M + \frac{1}{7!}(D^6\mathbf{u})_M + \cdots - \mathbf{v}_M\right] \qquad [3]$$

where

$$\mathbf{K} = 16\pi abc\left(\frac{\mathbf{i}'\mathbf{i}'}{\chi_0 + a^2\alpha_0} + \frac{\mathbf{j}'\mathbf{j}'}{\chi_0 + b^2\beta_0} + \frac{\mathbf{k}'\mathbf{k}'}{\chi_0 + c^2\gamma_0}\right),$$

$$\chi_0 = abc\int_0^\infty \frac{d\lambda'}{\Delta},$$

$$\alpha_0 = abc\int_0^\infty \frac{d\lambda'}{(a^2 + \lambda')\Delta},$$

$$\beta_0 = abc\int_0^\infty \frac{d\lambda'}{(b^2 + \lambda')\Delta},$$

$$\gamma_0 = abc\int_0^\infty \frac{d\lambda'}{(c^2 + \lambda')\Delta},$$

$$\Delta = [(a^2 + \lambda')(b^2 + \lambda')(c^2 + \lambda')]^{1/2},$$

and

$$D^2 = a^2\frac{\partial^2}{\partial x'^2} + b^2\frac{\partial^2}{\partial y'^2} + c^2\frac{\partial^2}{\partial z'^2}.$$

The moment $\mathbf{T}_{M,F}$ acting on an ellipsoidal particle under the above specified conditions of motion has been calculated first by Jeffery (3) to be

$$\begin{pmatrix} T_{M,F,x'} \\ T_{M,F,y'} \\ T_{M,F,z'} \end{pmatrix} = \begin{pmatrix} \frac{16\pi\mu abc}{3(b^2\beta_0 + c^2\gamma_0)}[(b^2 - c^2)f' + (b^2 + c^2)(\xi' - \omega_{x'})] \\ \frac{16\pi\mu abc}{3(c^2\gamma_0 + a^2\alpha_0)}[(c^2 - a^2)g' + (c^2 + a^2)(\eta' - \omega_{y'})] \\ \frac{16\pi\mu abc}{3(a^2\alpha_0 + b^2\beta_0)}[(a^2 - b^2)h' + (a^2 + b^2)(\zeta' - \omega_{z'})] \end{pmatrix} \qquad [4]$$

and recently, by Brenner (2), to be

$$\mathbf{T}_{M,F} = \mu\mathbf{Q}\left[(\Box x\mathbf{u})_M + \frac{3!2}{5!}(D^2\Box x\mathbf{u})_M + \frac{3!3}{7!}(D^4\Box x\mathbf{u})_M + \cdots - (a_{i+1}{}^2 + a_{i+2}{}^2)\boldsymbol{\omega}\right] \qquad [5]$$

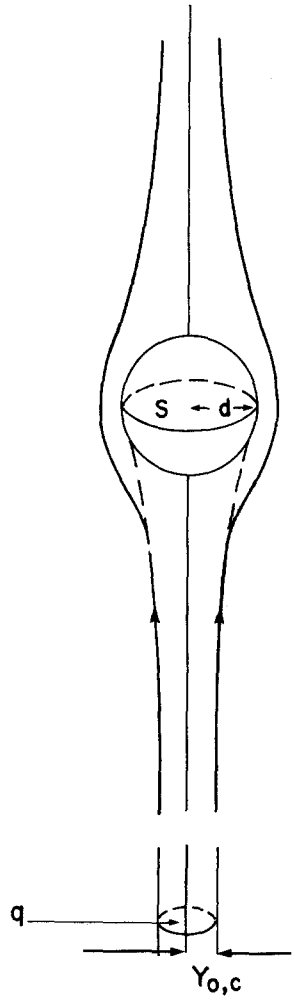

FIG. 1. Particle's limiting trajectory (schematical case). $E = q/S = (y_{0,c}/d)^2$.

where α_0, β_0, γ_0 are the above-defined integrals; f', g', h' are the fluid-strain coefficients, respectively, defined by $f' = \frac{1}{2}(\partial w'/\partial y' + \partial v'/\partial z')$, $g' = \frac{1}{2}(\partial u'/\partial z' + \partial w'/\partial x')$, and $h' = \frac{1}{2}(\partial v'/\partial x' + \partial u'/\partial y')$; ξ', η', ζ' are the vorticity coefficients, all expressed in a system of coordinates attached to the ellipsoid and parallel to its principal axes. $\mathbf{Q}$ is defined by

$$\mathbf{Q} = \frac{16\pi abc}{3}\left(\frac{\mathbf{i}'\mathbf{i}'}{b^2\beta_0 + c^2\gamma_0} + \frac{\mathbf{j}'\mathbf{j}'}{c^2\gamma_0 + a^2\alpha_0} + \frac{\mathbf{k}'\mathbf{k}'}{a^2\alpha_0 + b^2\beta_0}\right);$$

the operator $\square$ is defined by

$$\square = \mathbf{i}'a^2\frac{\partial}{\partial x'} + \mathbf{j}'b^2\frac{\partial}{\partial y'} + \mathbf{k}'c^2\frac{\partial}{\partial z'};$$

and $(a_{i+1}^2 + a_{i+2}^2)\boldsymbol{\omega} = (b^2 + c^2)\omega_{x'}$ for $T_{M,F,x'}$, $(a_{i+1}^2 + a_{i+2}^2)\boldsymbol{\omega} = (c^2 + a^2)\omega_{y'}$ for $T_{M,F,y'}$, etc. It should be pointed out that Eqs. [4] and [5] differ from each other only in the $\mathbf{u}_M$-velocity dependent terms beyond the first.

To solve the equations of motion near a collecting surface, one needs to know also the field of flow $\mathbf{u}(\mathbf{r},t)$; thus, once this is obtained, the trajectories of the particles can be essentially calculated whether analytically or numerically for various initial conditions. From this calculation it is possible to get the limiting paths confining a subspace out which all incoming particles collide with the obstacle in question (Fig. 1). The effectiveness of the collision process is expressed by the so called collision efficiency E which is defined as the ratio between the subspace cross-section in the initial direction of particle motion and some geometric cross-section of the collecting obstacle in that direction (Fig. 1), or the so-called linear collision efficiency which is the square root of the former.

Concerning the ellipsoidal shape, it is surely an ideal form not met with in nature; however, ellipsoids are frequently taken as a parent model for real particles. Thus, long cylinders such as asbestos and glass fibers, cloud ice needles, or even the carbon fibers which are being introduced into modern technology, may be simulated by elongated prolate spheroids while platelet-like particles may be approximated by oblate ellipsoids.

Previous Studies

Aerosol systems having nonspherical particles are as abundant as those containing spherical droplets. Nevertheless, whereas there is an enormous number of studies on the collision mechanism in the latter kind of systems (4), this process in the former kind has not been much investi-

gated either from a theoretical or from an experimental point of view. Some experimental studies on nonspherical particles have been performed though on the basis of the aerodynamic radius concept in which it was assumed that particles of identical aerodynamic radius have the same impaction characteristics (5); however, recent investigations on that radius have shown the inherent limitations of the concept (6, 7).

II. AIM OF STUDY

Due to the practical importance of the inertial collision process in the case of nonspherical particles and, essentially, the nonexistence of theoretical studies on the subject, we thought it worthwhile to calculate the efficiency of collision in significant cases.

We chose to deal first with a system of a spherical droplet falling through an aerosol consisting of (prolate) spheroidal needles in a medium at rest at infinity. The spherical particle was meant to represent scavenging rain or scrubber droplets while the spheroidal needles were imagined to simulate asbestos fibers, which are found to be in a nonnegligible concentration in the atmosphere (8), or even straight-chain aggregates of isometric primary particles.

The inertial collision efficiency was intended to be studied as a function of the dimensions of the spheroidal needles for typical, realistic size cases (8) in which Brownian translation and rotation can be neglected as judged by order of magnitude estimates (see further in text). These cases were considered by us to cover a partial though quite important part of the spectrum of sizes which are large enough to be treated deterministically and whose rate of fall in the atmosphere is still significantly small (6).

The calculational method we aimed to establish was meant to apply to any particle of a general ellipsoid form which may represent various encountered types of aerosol systems.

III. MATHEMATICAL MODEL AND METHOD OF CALCULATION

Systems of Coordinates

In dealing with our problem, we mainly used two systems of right-handed cartesian coordinates (Fig. 2). The first (x,y,z) was attached to the collecting droplet with its z axis parallel to the direction of gravity but pointing upward, and the second (x',y',z') was bound to the spheroidal particle itself with its y' axis along the pole of the ellipsoid.

To specify the orientation of the particle, we employed the so-called Euler angles ϕ, θ, and ψ, depicted in Fig. 2. So, in this way, components of any vector $\mathbf{P}$ in the first and second system were related according to

$$\mathbf{P} = \mathbf{A}^{-1}\mathbf{P}' \qquad [6]$$

where the transformation matrix $\mathbf{A}^{-1}$ is given by

$$\mathbf{A}^{-1} = \begin{pmatrix} \cos\psi\cos\phi - \cos\theta\sin\theta\sin\psi & -\sin\psi\cos\theta - \cos\theta\sin\phi\cos\psi & \sin\theta\sin\phi \\ \cos\psi\sin\phi + \cos\theta\cos\phi\sin\psi & -\sin\psi\sin\phi + \cos\theta\cos\phi\cos\psi & -\sin\theta\cos\phi \\ \sin\theta\sin\psi & \sin\theta\cos\psi & \cos\theta \end{pmatrix}. \qquad [7]$$

Restrictions and Assumptions

In constructing the mathematical model for our calculations, we have restricted ourselves first to particle motions in the so-called continuous medium, which limited the sizes considered to those befitting $K_n \ll 1$. Second, we confined ourselves, with no loss of generality, to prolate ellipsoids of the micron size range, and to a collecting droplet of the tens of micron range which falls under the action of gravity alone in a medium at rest at infinity. Thus, neglecting the effect of the fluid dynamic

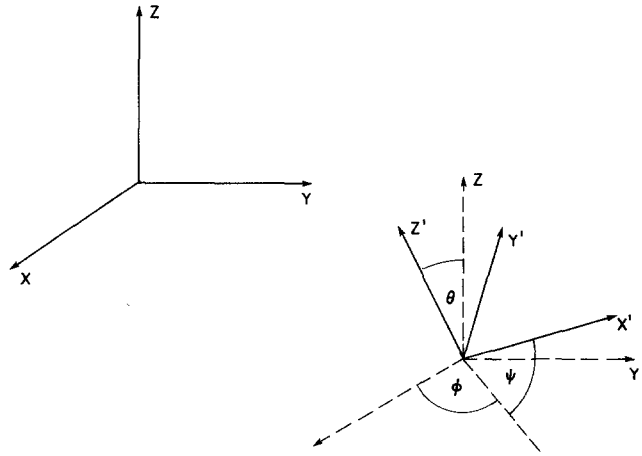

FIG. 2. The two systems of coordinates.

disturbance produced by our small particles on the large collecting droplet, we replaced our physical situation by that in which the x, y, z coordinate system became the main (inertial) system and the medium at infinity moved in the positive z direction with a velocity $|\mathbf{u}| = |\mathbf{v}_{M,\infty}|$ identical with the terminal rate of fall of the droplet.

Concerning the motion of the ellipsoidal particle, it was assumed to occur under quasistationary creeping flow conditions in which its instantaneous aerodynamic behavior is similar to that in a steady state of the same momentary characteristics. Thus, the effect of the time-dependent terms in the (linearized) Navier–Stokes equation on the force $\mathbf{F}_F$ and torque $\mathbf{T}_{M,F}$, was neglected. In other words, we have adhered to the procedure commonly used in aerosol physics that, in calculating the linear and angular acceleration of the particle (Eqs. [1] and [2]), one can still use Eqs. [3] and [4]. Obviously, the smaller these accelerations are, the better the assumption will hold; however, the degree of exactness involved with it can be assessed only by experiment.

As a first approximation, we have disregarded the wall effect produced by the fluid dynamic interaction between the ellipsoid and the droplet (see Discussion). So, the force $\mathbf{F}_F$ and torque $\mathbf{T}_{M,F}$ acting on the former were calculated as if the field of flow $\mathbf{u}$ was created by the presence of the droplet alone. This may be quite reasonable for particle-droplet separations greater than about 10 typical particle lengths, and even satisfactory for smaller distances (9). At intervening gaps of the order of or smaller than a mean free gaseous path, the continuous fluid assumption would break down anyway (10). At such gaps, an increase in the resistance of the fluid to the particle's approach toward the wall, which might have been the sole change if the medium could be considered continuous right to the surface, will be much reduced due to the prevailing rarified gas conditions. One should remember also that particle trajectories in the inertial collision process are determined by the external and fluid dynamic forces operating along the *whole* path, which has been the rationale for neglecting surface proximity effects whose contribution was thought to be of a second order (4).

Working Equations of Motion

Taking the case where gravity is the only operating external force and where the particles are homogeneously dense, we had, instead of Eqs. [1] and [2],

$$m d\mathbf{v}_M/dt = m\mathbf{g} + \mathbf{F}_F \qquad [8]$$

and

$$d(\mathbf{I}_M \cdot \boldsymbol{\omega})/dt = T_{m,F}. \quad [9]$$

Here, the translational motion given by Eq. [8] was considered in the inertial coordinate system attached to the collecting droplet while the rotational motion, expressed in [9], was regarded in the x', y', z' (second) system. Thus, whereas Eq. [8] was kept in its original form, Eq. [9] had to be converted to the so-called Euler's set of equations

$$I_{x'x'}d\omega_{x'}/dt - \omega_{y'}\omega_{z'}(I_{y'y'} - I_{z'z'}) = T_{M,F,x'}, \quad [10]$$

$$I_{y'y'}d\omega_{y'}/dt - \omega_{z'}\omega_{x'}(I_{z'z'} - I_{x'x'}) = T_{M,F,y'}, \quad [11]$$

and

$$I_{z'z'}d\omega_{z'}/dt - \omega_{x'}\omega_{y'}(I_{x'x'} - I_{y'y'}) = T_{M,F,z'} \quad [12]$$

in which the second term on the left of [11] was zero since $I_{x'x'} = I_{z'z'}$ for our prolate ellipsoids.

The translational resistance $\mathbf{F}_F$ was given by

$$\mathbf{F}_F = \mu\mathbf{K}\cdot(\mathbf{u}_M - \mathbf{v}_M) \quad [13]$$

which stems from Eq. [3] after neglecting the mid-terms in the latter.[4] Thus, Eq. [13] could be written in its components form as

$$\mathbf{F}_F = \begin{pmatrix} F_{F,x} \\ F_{F,y} \\ F_{F,z} \end{pmatrix} = \mu \begin{pmatrix} \mathbf{i}\cdot\mathbf{K}\cdot(\mathbf{u}_M - \mathbf{v}_M) \\ \mathbf{j}\cdot\mathbf{K}\cdot(\mathbf{u}_M - \mathbf{v}_M) \\ \mathbf{k}\cdot\mathbf{K}\cdot(\mathbf{u}_M - \mathbf{v}_M) \end{pmatrix}$$

$$= \mu \left\{ \begin{pmatrix} \sum_{i=1}^{3} f_{1i}^2 K_{ii} \\ \sum_{i=1}^{3} f_{1i}f_{2i}K_{ii} \\ \sum_{i=1}^{3} f_{1i}f_{3i}K_{ii} \end{pmatrix} (u_{M,x} - v_{M,x}) \right.$$

$$+ \begin{pmatrix} \sum_{i=1}^{3} f_{2i}f_{1i}K_{ii} \\ \sum_{i=1}^{3} f_{2i}^2 K_{ii} \\ \sum_{i=1}^{3} f_{2i}f_{3i}K_{ii} \end{pmatrix} (u_{M,y} - v_{M,y})$$

$$\left. + \begin{pmatrix} \sum_{i=1}^{3} f_{3i}f_{1i}K_{ii} \\ \sum_{i=1}^{3} f_{3i}f_{2i}K_{ii} \\ \sum_{i=1}^{3} f_{3i}^2 K_{ii} \end{pmatrix} (u_{M,z} - v_{M,z}) \right\} \quad [14]$$

where

$$(f_{ij}) = (A^{-1}). \quad [15]$$

The fluid dynamic torque $\mathbf{T}_{M,F}$ was expressed by Eq. [4], and the components of the moment of inertia by

$$\begin{pmatrix} I_{x'x'} \\ I_{y'y'} \\ I_{z'z'} \end{pmatrix} = m \begin{pmatrix} \frac{a^2 + b^2}{5} \\ \frac{2a^2}{5} \\ \frac{a^2 + b^2}{5} \end{pmatrix}. \quad [16]$$

The diagonal components of the translation tensor $\mathbf{K}$ for our ellipsoids were given in (11)

$$K_{11} = K_{33} = 6\pi a(8/3)(\beta^2 - 1)\Big/\left[\frac{2\beta^2 - 3}{(\beta^2 - 1)^{1/2}} \times \ln\langle\beta + (\beta^2 - 1)^{1/2}\rangle + \beta\right] \quad [17]$$

and

$$K_{22} = 6\pi a(4/3)(\beta^2 - 1)\Big/\left[\frac{2\beta^2 - 1}{(\beta^2 - 1)^{1/2}} \times \ln\langle\beta + (\beta^2 - 1)^{1/2}\rangle - \beta\right] \quad [18]$$

[4] This was found to be justified in our cases.

where K_{11}, K_{22}, K_{33} are the components along the x', y', z' axes, respectively (Fig. 2), and $\beta = (b/a) > 1$. Likewise, the integrals designated in Eq. [4] and the expression for **Q** by α_0, β_0, and γ_0, took in our case the form

$$\alpha_0 = \gamma_0 = a^2 b \int_0^\infty \frac{d\lambda'}{(a^2 + \lambda')^2 (b^2 + \lambda')^{1/2}}$$

$$= \frac{b^2}{(b^2 - a^2)} + \frac{a^2 b}{2(b^2 - a^2)^{3/2}} \times \ln \left\langle \frac{b - (b^2 - a^2)^{1/2}}{b + (b^2 - a^2)^{1/2}} \right\rangle \quad [19]$$

and

$$\beta_0 = bc^2 \int_0^\infty \frac{d\lambda'}{(c^2 + \lambda')(b^2 + \lambda')^{3/2}}$$

$$= -\frac{2c^2}{(b^2 - c^2)} - \frac{bc^2}{(b^2 - c^2)^{3/2}} \times \ln \left\langle \frac{b - (b^2 - c^2)^{1/2}}{b + (b^2 - c^2)^{1/2}} \right\rangle . \quad [20]$$

The translational equations of motion of the prolate ellipsoid were nondimensionalized by introducing

$$\mathbf{v}_M^* = \mathbf{v}_M / |\mathbf{v}_{M,\infty}|, \quad \mathbf{u}^* = \mathbf{u}_M / |\mathbf{v}_{M,\infty}|,$$

and

$$t^* = t/(d/|\mathbf{v}_{M,\infty}|)$$

where $\mathbf{v}_{M,\infty}$ is the terminal velocity of the droplet. Thus, from Eqs. [8] and [14], we got

$$dv_{M,x}^*/dt^* = -c_k \{ [\sum_{i=1}^{3} f_{1i}^2 K_{ii}](v_{M,x}^* - u_{M,x}^*) + [\sum_{i=1}^{3} f_{1i} f_{2i} K_{ii}](v_{M,y}^* - u_{M,y}^*) + [\sum_{i=1}^{3} f_{1i} f_{3i} K_{ii}](v_{M,z}^* - u_{M,z}^*) \}, \quad [21]$$

$$dv_{M,y}^*/dt^* = -c_k \{ [\sum_{i=1}^{3} f_{2i} f_{1i} K_{ii}](v_{M,x}^* - u_{M,x}^*) + [\sum_{i=1}^{3} f_{2i}^2 K_{ii}](v_{M,y}^* - u_{M,y}^*) + [\sum_{i=1}^{3} f_{2i} f_{3i} K_{ii}](v_{M,z}^* - u_{M,z}^*) \}, \quad [22]$$

and

$$dv_{M,z}^*/dt^* = -c_k \{ [\sum_{i=1}^{3} f_{3i} f_{1i} K_{ii}](v_{M,x}^* - u_{M,x}^*) + [\sum_{i=1}^{3} f_{3i} f_{2i} K_{ii}](v_{M,y}^* - u_{M,y}^*) + [\sum_{i=1}^{3} f_{3i}^2 K_{ii}](v_{M,z}^* - u_{M,z}^*)] \} - \frac{|\mathbf{g}| d}{|\mathbf{v}_{M,\infty}|^2} \quad [23]$$

where

$$c_k = 3\mu d / 4\pi a^2 b |\mathbf{v}_{M,\infty}| \rho_1.$$

The rotational equations, however, were kept in their dimensional form.

Field of Flow

The velocity of the fluid **u** in our case of small particles streaming past a much larger droplet was taken to be essentially given by the field of flow around an isolated solid sphere. This two-dimensional field has been previously generated by us (12), as well as by others (13), by a numerical solution of the Navier–Stokes equation for a steady state; we used now two-dimensional grids of stream function and vorticity values characterized by an angular separation ($\Delta\theta'$) and a radial distance (R) amounting to 6° and $e^{0.10472 \cdot N}$ or 3° and $e^{(0.10472/2)N}$, respectively, though later we returned to the first type of grid because of physical considerations (see Results). As the velocity $\mathbf{u}(u_\rho, u_z)$ of this field is axisymmetric, its resolutes in the droplet's coordinate system could be expressed by

$$\mathbf{u} = \begin{pmatrix} u_x \\ u_y \\ u_z \end{pmatrix} = \begin{pmatrix} u_\rho \cdot x/\rho \\ u_\rho \cdot y/\rho \\ u_z \end{pmatrix} \quad [24]$$

where $\rho = (x^2 + y^2)^{1/2}$. The values of these components between the grid points were computed according to a linear interpolation.

Cases of Particle's Motion

We classified the motion of our particles into two cases:

(i) Motion with meridianal symmetry, in which the rotational axis of the particles, y', lay in a meridianal plane of the collecting droplet.

(ii) Motion in an arbitrary orientation.

In the first case, we had, out of symmetry considerations, that $T_{M,F,y'} = T_{M,F,z'} = 0$, and, hence, $\omega_{y'} = \omega_{z'} = 0$ when $\omega_{x',0} = \omega_{y',0} = \omega_{z',0} = 0$. Thus, Eqs. [10]–[12] did turn into

$$I_{x'x'}d\omega_{x'}/dt = T_{M,F,x'} = A_1 - B_1\omega_{x'} \quad [25]$$

where

$$\omega_{x'} = d\theta/dt \quad [26]$$

and A_1, B_1 are local functions of the flow field and the dimensions of the ellipsoid (Eq. [4]).

In the second case, we had to use intact Eqs. [10] through [12], which could be written as (Eqs. [4])

$$I_{x'x'}d\omega_{x'}/dt - \omega_{y'}\omega_{z'}(I_{y'y'} - I_{z'z'}) = A_1 - B_1\omega_{x'} \quad [27]$$

$$I_{y'y'}d\omega_{y'}/dt = A_2 - B_2\omega_{y'}, \quad [28]$$

and

$$I_{z'z'}d\omega_{z'}/dt - \omega_{x'}\omega_{y'}(I_{x'x'} - I_{y'y'}) = A_3 - B_3\omega_{z'} \quad [29]$$

where A_2, B_2, A_3, B_3 are also functions of the flow field and the geometry of the ellipsoid (4). The relationships between $\omega_{x'}$, $\omega_{y'}$, $\omega_{z'}$ and the orientation angles ϕ, θ, and ψ are given by (14)

$$\omega_{x'} = \dot{\phi}\sin\theta\sin\psi + \dot{\theta}\cos\psi, \quad [30]$$

$$\omega_{y'} = \dot{\phi}\sin\theta\cos\psi - \dot{\theta}\sin\psi, \quad [31]$$

and

$$\omega_{z'} = \dot{\phi}\cos\theta + \dot{\psi} \quad [32]$$

which, once the components of the angular velocity are found, form a set of three linear equations for $\dot{\phi}$, $\dot{\theta}$, and $\dot{\psi}$.

Mathematical Procedure of Calculation

The method of calculation was based on treating the motion as a sequence of consecutive pairs of steps. In the first step, our ellipsoidal particle was assumed to translate for a sufficiently short time interval Δt in a fixed orientation (ϕ,θ,ψ) whereas in the second it was taken to rotate for an equal interval with no translation. Physically, this is based on the decoupling between the translational and rotational motion of the particle.

The calculational algorithm consisted of the following stages:

(1) Assigning initial values for particle location and orientation, viz., $x = x_0 = 0$, $y = y_0$, $z = z_0$, $\phi = \phi_0$, $\theta = \theta_0$, and $\psi = \psi_0$; also, choosing initial values for the particle's translational and rotational velocities, viz., $v_{M,x}^* = v_{M,y}^* = 0$, $v_{M,z}^* = 1$, $\omega_{x'} = \omega_{y'} = \omega_{z'} = 0$.

(2) Solving the equations of particle translation (Eqs. [21]–[23]) according to a fourth-order Runge–Kutta method with a properly adjustable time interval.

(3) Checking for occurrence of collision as the intercenter distance between the droplet and the ellipsoidal particle becomes $\rho < b + d$ (Appendix).

(4) Solving for the interval Δt the equations of particle rotation ([25] or [27]–[29]) by a fourth-order Runge–Kutta method, and getting the new orientation angles either directly (case i) or through Eqs. [30] to [32] (case ii), all while employing the local strain coefficients and vorticity components.

(5) Return to stage 2 and continuation of the cycle till collision ($s \leq s_c$), or until our particle overshoots the droplet and reaches $z^* = 20$.

In the equations of translation we used for the nth step the relationship

$$(f_{ij})_n = (A^{-1})_{n-1} \quad [33]$$

where $(A^{-1})_{n-1}$ pertains to orientation angles ϕ_{n-1}, θ_{n-1}, and ψ_{n-1} at the *beginning* of the step. The angles for the next, $(n + 1)$th, translational step were obtained from their time derivatives at the *end* of the nth step according to the relationships $\phi_n \cong \phi_{n-1} + \dot{\phi}\Delta t$, $\theta_n \cong \theta_{n-1} + \dot{\theta}\Delta t$, and $\psi_n \cong \psi_{n-1} + \dot{\psi}\Delta t$, as needed for case (i) or (ii). These angles were introduced into the transformation matrix.

The derivatives of the fluid velocity in the ellipsoid's coordinate system, $\partial u_{i'}/\partial x_{j'}$, needed for the evaluation of the strain coefficients and vorticity components which appear in Eq. [4], were given in terms of the derivatives in the droplet's set of coordinates by the similarity transformation

$$(\partial u_{i'}/\partial x_{j'}) = \mathbf{A}(\partial u_{k'}/\partial x_l)\mathbf{A}^{-1} \qquad [34]$$

where $u_{i'} = (u',v',w')$, $x_{j'} = (x',y',z')$, $u_{k'} = (u,v,w)$ and $x_l = (x,y,z)$. The velocity derivatives in the droplet's coordinate system, $\partial u_{k'}/\partial x_l$ were found from our flow field solution by a finite difference technique exemplified in

$$\partial u_i/\partial x_l = \frac{\sigma_1 u_{i+1}, \cdots - \sigma_2 u_i, \cdots}{\Delta x_l} \qquad [35]$$

where σ_1 and σ_2 are weights derived from the position of particle's center in the flow field grid, and $\sigma_1 + \sigma_2 = 1$.

IV. PARAMETERS

The constant parameters used in the calculations were:

(1) Viscosity of gaseous medium, 1.718×10^{-4}cgs, which is the appropriate value for air at 900 mb and 0°C (15).

TABLE I

Dimensions of the Ellipsoidal Particles

	b (μm)	
a (μm)	5	10
0.5	Case 1	Case 3
1	Case 2	Case 4

TABLE II

The Effect of the Integration Step-Time Interval and the Density of the Droplet[a]

a (μm)	b (μm)	ϕ_0	θ_0	ψ_0	$\lvert Z_0^* \rvert$[5]	ρ_1(g·cm^{-3})	Δt^*	$E_1 \times 10^2$
						1	*A*	6.94
			$\pi/4$				*B*	8.27
1	10	0		0	64	2.23	*A*	9.06
							B	8.97

[a] *A*, $\Delta t^* = 0.1$ for $R > 1.5$; $\Delta t^* = 0.05$ for $R \leq 1.5$. *B*, $\Delta t^* = 0.05$ for $R > 1.5$; $\Delta t^* = 0.025$ for $R \leq 1.5$. Characteristics of flow field grid: $\Delta\theta' = 6°, R = e^{0.10472 \cdot N}$; radius of collecting droplet, 75 μm.

(2) Gravitational acceleration, 981 cm sec^{-2}.

(3) Particle's density, 1, and 2.23 g cm^{-3} which is the value for glass fibers (16).

(4) Droplet's density, 1 g cm^{-3}.

The dimensions of the (prolate) spheroidal particles studied are given in Table I. The radius of the collecting droplet was 75 μm, which makes the Reynolds number of its terminal rate of fall 4.87.

Obviously, these dimensions do not extend over the whole range of atmospheric, industrial, or laboratory particles and droplets; however, we thought that the calculated cases presented here will bring out the pertinent features of the collisional process between elongated particles and spheres.

V. RESULTS

The calculations were performed with the aid of the Hebrew University CDC CYBER 74 computer. The trajectories of our particles were computed for various initial conditions of the horizontal separation, thus furnishing the critical value $y_{0,c}$ (Fig. 1) which defines the limiting path and determines the linear collision efficiency $E_l = y_{0,c}/d$. At these initial conditions, our droplet's coordinate system was set so that we had always $x_0 = 0$. The critical value $y_{0,c}$ was found by taking the arithmetic

[5] $\lvert z_0^* \rvert = 64$ is approximately equivalent to $\lvert z^* \rvert = e^{40 \cdot Be} - 2$.

TABLE III

The Effect of the Initial Vertical Separation[a]

a (μm)	b (μm)	ϕ_0	θ_0	ψ_0	$\lvert Z_0^* \rvert$	$E_1 \times 10^2$
					11.7	8.47
1	10		$\pi/4$		21.2	9.31
		0		0	48.8	10.31
					57.4	10.69
					64	9.06

[a] Δt^*, A; $\rho_1 = 2.23$ g cm^{-3}; characteristics of flow field grid, $\Delta\theta' = 6°$; $R = e^{0.10472.N}$; radius of collecting droplet, 75 μm.

average of the $y_{0,1}$ value pertaining to the closest overshooting and collision trajectories. The relative accuracy in this procedure, $\Delta E/\bar{E} = |y_{0,c} - y_{0,1}|/\bar{E}$, was about 0.005 to 0.01, which was considered to be sufficient.

Preliminary tests

As a preliminary check, we investigated the effect on the collision efficiency of the step-time interval, the density of the particle, the initial vertical separation, and the field of flow resolution.

(i) Step-time interval and particle's density. The effect of the step-time interval used in the integration of the equations of motion as well as the effect of particle density are shown in Table II for otherwise constant conditions.

From this table one can perceive that the linear collision efficiencies for time schedule A and B differ by 19.2% when $\rho_1 = 1$ g cm^{-3}, and by 0.99% when $\rho_1 = 2.23$ g cm^{-3} which may be ignored; likewise, one can note that the effect of the change in density is about 30.5% for time schedule A and about 8.5% for time schedule B (see Discussion).

(ii) Initial vertical separation. The influence of the initial vertical separation on the collisional efficiency is shown in Table III and Fig. 3 for otherwise constant conditions. Here, one can observe the (unexpected) existence of a slight maximum of E_l which does not appear in the case of two spherical particles where E_l monotonically decreases with z_0^* (12) (see Discussion).

(iii) Field of flow resolution. The effect of the resolution in the numerically calculated field of flow on E is shown in Table IV for a few cases. From this table it can be noted that, in contrast with the influence of the other parameters, that of the flow resolution is quite important. Naturally, one is tempted

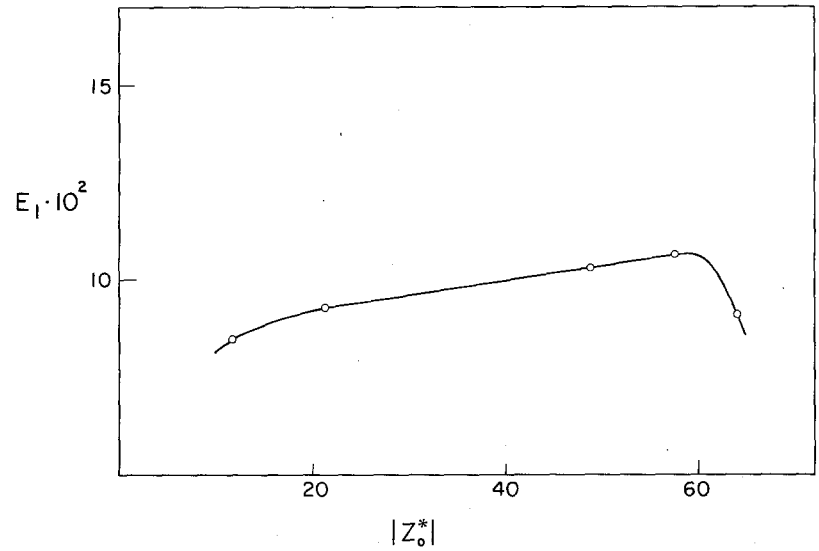

FIG. 3. The effect of the initial vertical separation (see Table III).

here to generate flow fields of increasing resolution and check for an asymptotic effect; however, it should be remembered that, from a *physical point* of view, the finer we make the grid of stream function and vorticity values, the more we deviate from the original assumptions of Jeffery (3) on which our entire calculations are based. According to these assumptions, the subspace enclosing our ellipsoid should be of constant fluid dynamic properties through a volume which is large compared with the dimensions of the particle. Thus, having to strike a compromise between the numerical calculation and the fluid dynamic demands, we adhered in the following calculations to flow resolution *C*.

TABLE IV

The Effect of the Resolution in the Calculated Field of Flow[a] and Characteristics of Flow Resolution[b]

a (μm)	b (μm)	θ_0	Flow grid	$E_1 \times 10$
		0	C	9.31
		$\pi/2$		8.22
1	10			
		0	D	13.62
		$\pi/2$		10.97

[a] $\phi_0 = \psi_0 = 0$; $\rho_1 = 2.23$ g cm^{-3}; $d = 75$ μm; step-time schedule, *A*.

[b] *C*, $\Delta\theta' = 6°$, $R = e^{Be \cdot N}$, 41 × 31 grid points; *D*, $\Delta\theta' = 3°$, $R = e^{(Be/2) \cdot N}$, 81 × 61 grid points.

Orderly vs Stochastic Behavior

In addition to the above checks, we tested the basis for our neglect of particle stochastic motion, especially in what concerns Brownian rotation vs the gradient rotation considered here. Thus, we computed in every calculational run the ratio α between the root-mean square of the change of our particle's orientation angle θ_B due to Brownian effects during a total time

$$t = \sum_n \Delta t_n,$$

and the sum of the (absolute) changes in angle

$$\sum_n |\Delta\theta_n|$$

in that (total) time due only to flow gradients.

This ratio is expressed by

$$\alpha = \frac{(\overline{\Delta\theta_B^2})^{1/2}}{\sum_n |\Delta\theta_n|} \qquad [36]$$

where the numerator is given in (17)

$$(\overline{\Delta\theta_B^2})^{1/2} = (2kTB_w t)^{1/2}, \qquad [37]$$

the rotational mobility of the prolate ellipsoid about its equatorial axis is (17)

$$B_w = \frac{3\left\{\dfrac{2\beta^2 - 1}{(\beta^2 - 1)^{1/2}} \ln \langle \beta + (\beta^2 - 1)^{1/2} \rangle - \beta\right\}}{16\pi a^3(\beta^4 - 1)}, \qquad [38]$$

k is Boltzmann's constant, and $T = 300$°K. The justification for ignoring Browning rotation was judged according to the magnitude of α.

The relative significance of the translational Brownian motion was checked too by comparing the root-mean-square of the (Brownian) displacement in a typical time to a distance which is traversed by our particle during that time in an orderly fashion and due to its inertia. A typical ratio between these distances for even an exaggerated stochastic motion was of the order of 10^{-4}, which makes ignoring the Brownian translation of our particles quite justifiable.

Collision Efficiency Calculations

The linear collision efficiencies calculated for various cases of interest are presented in Tables V through VII and Figs. 4 through 6. Some typical particle trajectories, show-

TABLE V

Linear Collision Efficiencies of Ellipsoidal Elongated Particles[a]

Dimension cases[b]		$E_1 \times 10^2$							
		$\theta_0 = 0$		$\theta_0 = \pi/4$		$\theta_0 = \pi/2$		$\theta_0 = 3\pi/4$	
1	3	4.03 ($\alpha = 0.021$)	7.19 ($\alpha = 0.004$)	3.94 ($\alpha = 0.007$)	7.06 ($\alpha = 0.005$)	3.36 ($\alpha = 0.008$)	6.06 ($\alpha = 0.003$)	4.47 ($\alpha = 0.006$)	7.66 ($\alpha = 0.003$)
2	4	4.97 ($\alpha = 0.034$)	9.31 ($\alpha = 0.058$)	4.71 ($\alpha = 0.006$)	9.06 ($\alpha = 0.005$)	3.32 ($\alpha = 0.007$)	8.22 ($\alpha = 0.002$)	5.69 ($\alpha = 0.006$)	10.22 ($\alpha = 0.002$)

[a] $\phi_0 = \psi_0 = 0$; $\rho_1 = 2.23$ g cm^{-3}; $d = 75$ μm, step-time schedule, A; flow field resolution, C; $|Z_0^*| = e^{40Be} - 2 \cong 64$.
[b] See Table I.

ing the orientation at various stages of the motion, are depicted in Figs. 7 and 8.

The results are given for the four dimension cases of Table I, and for various initial orientation angles. In real situations, of course, these orientations may be distributed according to a certain function. Thus, the average efficiency figure for each pair of an ellipsoidal elongated particle and a droplet would have to be deduced from our calculated efficiencies by a proper probability weighing. For example, in the case of a random initial orientation of identical elongated spheroids, the average linear efficiency would be expressed by

$$\bar{E}_l = \int_0^{2\pi}\int_0^{2\pi}\int_0^{\pi} E_l(\phi_0,\theta_0,\psi_0,a,b,d) \times \Phi(\phi_0,\theta_0,\psi_0)d\theta_0 d\phi_0 d\psi_0 \quad [39]$$

where the (random) probability density is given in

$$\Phi(\phi_0,\theta_0,\psi_0)d\theta_0 d\phi_0 d\psi_0 = (1/8\pi^2)\sin\theta_0 d\theta_0 d\phi_0 d\psi_0. \quad [40]$$

VI. DISCUSSION

General

In discussing our model, assumptions, and results, we find it convenient to frequently draw a comparison between the behavior of the nonspherical and spherical particles.

First, we should point out the essential difference between the treatments of the impaction process in the two cases. Thus, whereas the rotation motion of spherical particles is usually neglected, this motion is taken into consideration in the nonspherical case.

Second, we should remark about the assumptions made in our mathematical model. We have used for the fluid dynamic force and torque which act on our particles the steady-state solution results though the whole motion of the particles is really nonsteady in character. This quasistationary procedure is very common in aerosol physics; its justification is based on order of mag-

TABLE VI

Linear Collision Efficiencies of Ellipsoidal Elongated Particles[a]

Dimension cases[b]		$E_1 \times 10^2$							
		$\theta_0 = 0$		$\theta_0 = \pi/4$		[c]$\theta_0 = \pi/2$		$\theta_0 = 3\pi/4$	
1	3	1.72 ($\alpha = 0.0005$)	3.19 ($\alpha = 0.002$)	3.06 ($\alpha = 0.07$)	5.69 ($\alpha = 0.005$)	3.36 ($\alpha = 0.008$)	6.06 ($\alpha = 0.003$)	3.06 ($\alpha = 0.03$)	5.81 ($\alpha = 0.008$)
2	4	3.91 ($\alpha = 0.005$)	5.31 ($\alpha = 0.003$)	3.16 ($\alpha = 0.02$)	6.56 ($\alpha = 0.03$)	3.32 ($\alpha = 0.007$)	8.22 ($\alpha = 0.002$)	3.22 ($\alpha = 0.008$)	6.66 ($\alpha = 0.004$)

[a] $\phi_0 = \pi/2$, $\psi_0 = 0$; $\rho_1 = 2.23$ g cm^{-3}; $d = 75$ μm; step-time schedule, A; flow field resolution, C; $|Z_0^*| = e^{40Be} - 2 \cong 64$.
[b] See Table I.
[c] This orientational case is equivalent to that of $\phi_0 = \psi_0 = 0$, $\theta_0 = \pi/2$.

TABLE VII

Linear Collision Efficiencies of Ellipsoidal Elongated Particles[a]

Dimension cases[b]		$E_1 \times 10^2$							
		$\theta_0 = 0$		$\theta_0 = \pi/4$		$\theta_0 = \pi/2$		$\theta_0 = 3\pi/4$	
1	3	4.19 ($\alpha = 0.1$)	7.25 ($\alpha = 0.009$)	4.31 ($\alpha = 0.01$)	7.62 ($\alpha = 0.004$)	3.06 ($\alpha = 0.02$)	5.69 ($\alpha = 0.004$)	3.94 ($\alpha = 0.008$)	6.94 ($\alpha = 0.003$)
2	4	5.06	9.44 ($\alpha = 0.004$)	5.47 ($\alpha = 0.008$)	10.41 ($\alpha = 0.003$)	3.06 ($\alpha = 0.01$)	6.58 ($\alpha = 0.002$)	4.56 ($\alpha = 0.009$)	8.56 ($\alpha = 0.003$)

[a] $\phi_0 = 0$, $\psi_0 = \pi/4$; $\rho_1 = 2.23$ g cm^{-3}; $d = 75$ μm, step-time schedule, A; flow field resolution, C; $|Z_0^*| = e^{40Be} - 2 \cong 64$.
[b] See Table I.

nitude estimates of the various terms in the fundamental Navier–Stokes equation whose solution provides the force and torque formulae. However, one may imagine that there could be cases in which the cumulative effect of the (small) neglected nonsteady terms will affect the whole trajectory of the particles. So, the final test of the quasistationary assumption must be furnished by experiments.

The force and torque expressions adopted by us were derived for isolated ellipsoids located far from walls, which is obviously a first approximation. The fluid dynamic effect of walls on the trajectories of nonspherical axisymmetric (slender) particles near various obstacles is currently studied by us. Preliminary theoretical and experimental results show the existence of an unaccounted as yet perpendicular component of particle velocity which is about 10% of the parallel velocity; the overall effect on the trajectories, though, has not been assessed.

Scope of Study

The range of the particles' and droplets' parameters reported here surely does not cover the interesting cases met in nature, industry, and the laboratory. However, we think that the presented investigated cases do convey the unique feature of the motion of elongated spheroidal needles near spherical surfaces.

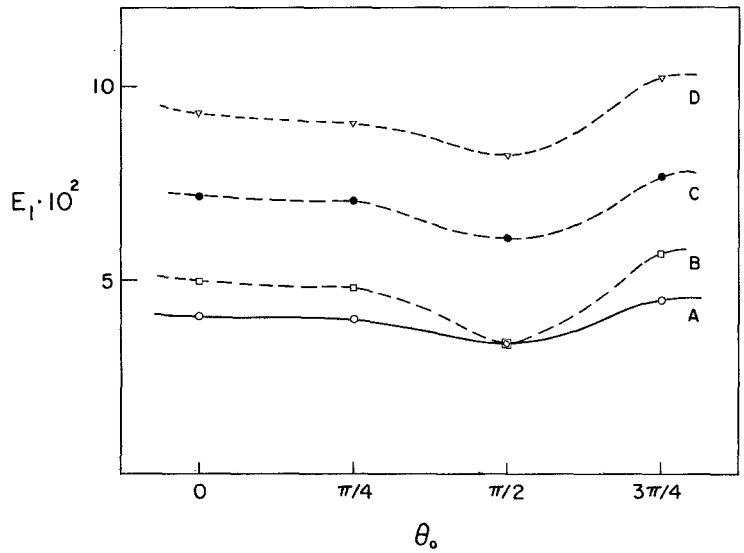

FIG. 4. The linear collision efficiency of ellipsoidal elongated particles vs θ_0 (see Table V). A, dimension case 1; B, dimension case 2; C, dimension case 3; D, dimension case 4.

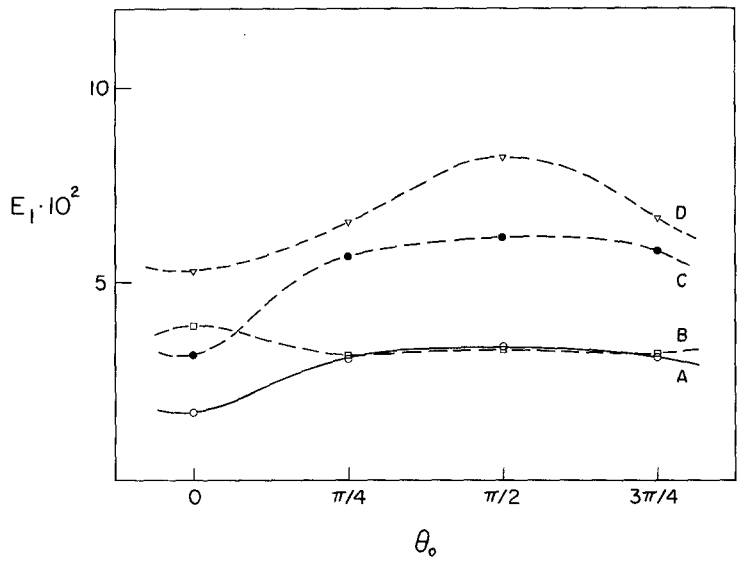

FIG. 5. The linear collision efficiency of ellipsoidal elongated particles vs θ_0 (see Table VI). A, dimension case 1; B, dimension case 2; C, dimension case 3; D, dimension case 4.

Also, the (pure) ellipsoidal shape which we used obviously does not exist in real situations. Nevertheless, we assume that it may simulate the behavior of approximately straight elongated particles.

Results

As mentioned above, in checking the effect of the initial vertical separation on the collision efficiency, we found a slight maximum in the E_l vs $|z_0^*|$ curve (Table III and Fig. 3); the range of E_l values actually extends to about $\pm 11.5\%$ of the average. This is contrary to the asymptotic decrease with separation usually encountered in the spherical case (12). Analyzing the orientation–location pattern of the tested particles from figures similar to Figs. 7 and 8, we

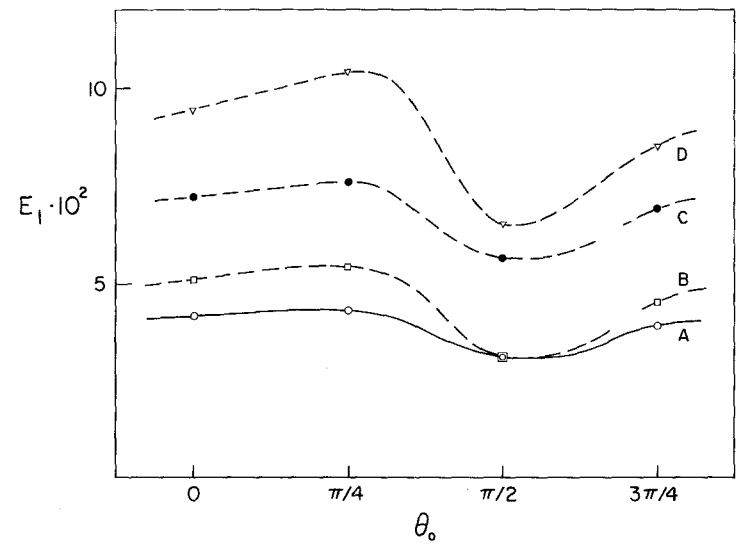

FIG. 6. The linear collision efficiency of ellipsoidal elongated particles vs θ_0 (see Table VII). A, dimension case 1; B, dimension case 2; C, dimension case 3; D, dimension case 4.

think that the behavior seen in Table III and Fig. 3 for $\theta_0 = \pi/4$, $\phi_0 = \psi_0 = 0$, stems from the very delicate interplay between the rotation of the particles, their translation, and the initial condition of their linear momentum, position, and orientation.

The effect of the flow field resolution discussed above brings out a case in which a compromise between computational and fluid dynamical demands has to be made.

Treating the collisional frequency data (Tables V–VII and Figs. 4–6), we use as gauges both the Froude's number,

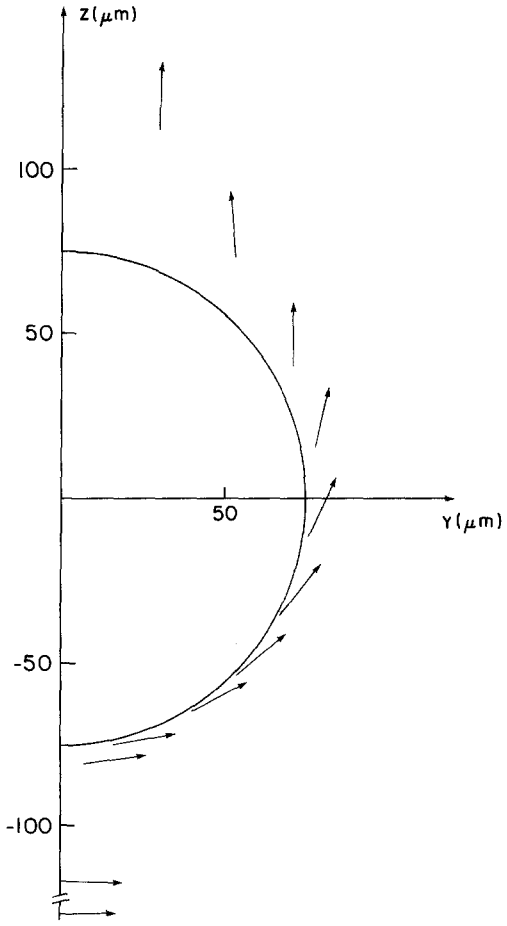

FIG. 7. The orientation of an ellipsoidal elongated particle at various stages of motion. $a = 1$ μm, $b = 10$ μm, $d = 75$ μm; $\theta_0 = 0$, $\phi_0 = \psi_0 = 0$; $|z_0^*| = e^{40 \cdot Be} - 2 \cong 64$; $y_{0,c} = 7.0312$ μm; step-time schedule—A; flow field resolution—C; $\rho_1 = 2.23$ g cm^{-3}.

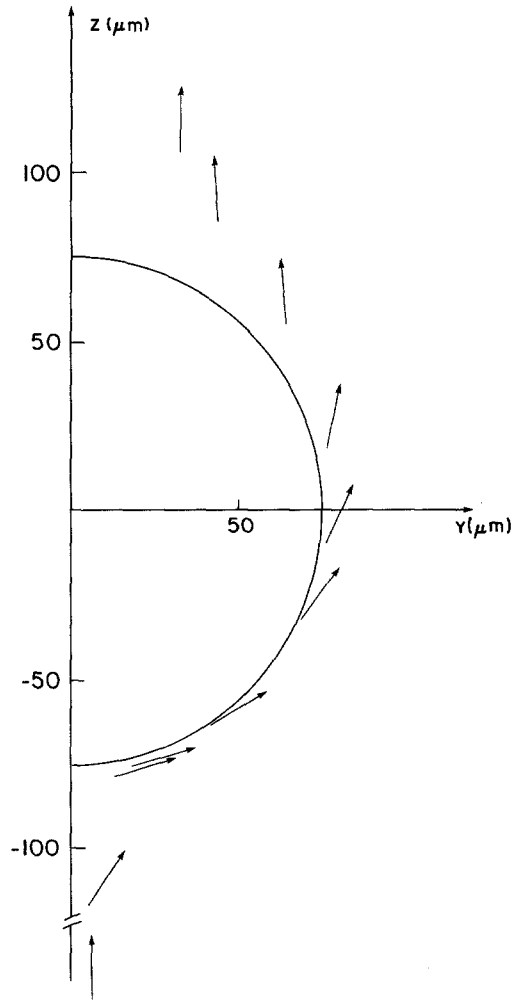

FIG. 8. The orientation of an ellipsoidal elongated particle at various stages of motion (see Fig. 7, except for: $\theta_0 = \pi/2$; $y_{0,c} = 6.1875$ μm).

$F_r (= |\mathbf{v}_{m,\infty}|^2/2|\mathbf{g}|d)$, and the Stokes' number based on the volumetrically equivalent radius R_1, Stk $(= m|\mathbf{v}_{M,\infty}|/6\pi\mu R_1 d)$. In the spherical case, particle collision efficiency is a monotonically increasing function of the Stokes' number for a constant F_r (4). However, here we see that it is not the usual occurrence. Thus, whereas the Stokes' number for our particles of the various dimension cases (Table I) increases in the order of case 1, case 3, case 2, and case 4, the linear collision efficiency E_l usually increases in the order of case 1, case 2, case 3,

and case 4 (Froude's number is a constant for all cases). This is another indication of the importance of the "steric" or orientational effect in the impaction process of our particles. Stokes number is clearly an insufficient general measure in our situation.

In the specific instance of $\phi_0 = \pi/2$, $\psi_0 = 0$, and $0 \leq \theta_0 \leq \pi/16$ approximately (Table VI and Fig. 5), we note, however, that E_l does increase with the increase of mass of the particles.

It is interesting to compare our results with those for spheres of equal volume. Thus, if we take the results of Grover *et al.* (18, Fig. 2) for a close enough spherical case of $\rho_1 = 2$ g cm^{-3} and $d = 72$ μm, we observe that the linear efficiency for a spherical particle equivalent to our particles of dimension cases 1, 2, 3, and 4 is 1.87×10^{-2}, 2.72×10^{-2}, 2.19×10^{-2}, and 6×10^{-2}, respectively. So, the ratio between our calculation efficiencies and their values is seen to be bounded from above by about 3.5 (case 3, $\phi_0 = \psi_0 = 0$, $\theta_0 = 3\pi/4$) and from below, by about 1. We think that this should be taken into consideration in real situations.

VII. SUMMARY

The equations describing the deterministic motion of an arbitrary aerosol particle in the inertial collision process have been formulated with due emphasis on particle rotation. The cases of ellipsoidal particles flowing past a spherical collector were treated and an appropriate algorithm devised. Indicative computations were performed for ellipsoidal needles simulating important types of aerosol systems. The method, however, is fit also to oblate shapes which approximate platelet-like (mineral) aerosol particles, and to any particle of the general ellipsoid form.

APPENDIX

The distance s between the surface of an ellipsoid

$$\frac{x'^2}{a^2} + \frac{y'^2}{b^2} + \frac{z'^2}{c^2} = 1 \qquad [1A]$$

and the surface of a sphere of radius d which is located at ξ^0, η^0, ζ^0 as expressed in the ellipsoidal system of coordinates, is given by

$$s = [(\xi^0 - x')^2 + (\eta^0 - y')^2 + (\zeta^0 - z')^2]^{1/2} - d. \qquad [2A]$$

To find the minimal value of s, we used the method of Lagrange's undetermined multipliers. Defining the functions $\varphi(x',y',z')$ and $F(x',y',z')$ by

$$\varphi(x',y',z') = \frac{x'^2}{a^2} + \frac{y'^2}{b^2} + \frac{z'^2}{c^2} - 1 \qquad [3A]$$

and

$$F(x',y',z') = (\xi^0 - x')^2 + (\eta^0 - y')^2 + (\zeta^0 - z')^2 - \lambda\varphi(x',y',z'), \qquad [4]$$

taking the partial derivatives of $F(x',y',z')$ with respect to x', y', z' and λ, and equating each one of these derivatives to zero, we got by the above method

$$\frac{x' - \xi^0}{(\partial\varphi/\partial x')} = \frac{y' - \eta^0}{(\partial\varphi/\partial y')} = \frac{z' - \zeta^0}{(\partial\varphi/\partial z')} = \frac{\lambda}{2}. \qquad [4A]$$

Thus, from the last equation and from [1A], we obtained a set of three equations for the three unknowns x', y', z'. Out of these equations we got for each of the unknowns a fourth-order polynomial which was numerically solved. The root giving after substitution in [2A] a minimal value of s was taken to be the relevant ones.

The vector (ξ^0,η^0,ζ^0) denoting the position of the droplet's center was found in our case from the position vector (x,y,z) of the ellipsoid's center in the droplet's set of coordinates according to the transformation

$$\begin{pmatrix} \xi^0 \\ \eta^0 \\ \zeta^0 \end{pmatrix} = \mathbf{A} \begin{pmatrix} -x \\ -y \\ -z \end{pmatrix}. \qquad [5A]$$

NOMENCLATURE

A_1–A_3, B_1–B_3	local functions of flow field (see text)
a, b, c	semiaxes of the ellipsoid ($a = c < b$)
$\mathbf{A}$	transformation matrix; $\mathbf{A}^{-1} = \mathbf{A}^t$, inverse of A
Be	= 0.10472
B_w	rotational mobility of a prolate ellipsoid about its equatorial axis
c_k	a parameter defined in text
$\mathbf{C}_R$	coupling tensor
d	radius of the collecting droplet
D^2	an operator defined in text
E	collision efficiency of the particle; $E_l = (E)^{1/2} = y_{0,c}/d$—linear collision efficiency
f', g', h'	fluid's strain coefficients, defined in text
$f_{i,j}$	direction cosine between the $x, y, z(i)$ and the $x', y', z'(j)$ coordinates
$\mathbf{F}$	force acting on the particle; $\mathbf{F}_e$—external force, $\mathbf{F}_F$—fluid dynamic force
$F(x',y',z')$	a function defined in text
$\mathbf{g}$	gravitational acceleration
$\mathbf{i}',\mathbf{j}',\mathbf{k}'$	unit vectors in ellipsoid's system of coordinates
$\mathbf{I}_M$	moment of inertia tensor about center of mass M
k	Boltzmann's constant
k'	dummy index
K_n	Knudsen's number (= mean free path of fluid molecules/typical particle's length)
$\mathbf{K}$	translation tensor
L	typical length of the particle
m	mass of the particle
n	index for time-step sequence
N	running index for radial distance in flow field grid
$\mathbf{P}, \mathbf{P}'$	position vector in the droplet's or the particle's system of coordinates, respectively
$\mathbf{Q}$	tensor, defined in text
$\mathbf{r}$	radius vector in field of flow's grid, r—absolute value
R	r/d, nondimensional
R_e^t	$= \lvert\mathbf{v}_M\rvert L/\nu$, translational Reynolds number
R_e^r	$= \lvert\boldsymbol{\omega}\rvert L^2/\nu$, rotational Reynolds number
s	distance between a surface point on the ellipsoid and on the collecting droplet
t	time, Δt—time interval; t^*—nondimensional time, defined in text
$\mathbf{T}_M$	torque about center of mass; $\mathbf{T}_{M,e}$—external torque, $\mathbf{T}_{M,F}$—fluid dynamic torque
T	temperature of medium (°K)
$\mathbf{u}$	fluid velocity; $\mathbf{u}_M$—fluid undisturbed velocity at the point occupied by particle's center of mass; $\mathbf{u}^*$—nondimensional velocity defined in text; u, v, w—velocity components
$\mathbf{v}_M$	translational velocity of the particle; $\mathbf{v}_M{}^*$—nondimensional velocity, defined in text; $v_{M,x}{}^*$, $v_{M,y}{}^*$, $v_{M,z}{}^*$—components along (inertial) axes x, y, and z, $\lvert\mathbf{v}_{M,\infty}\rvert$—terminal velocity of the droplet
x, y, z	inertial cartesian system of coordinates attached to collecting droplet
x', y', z'	particle-attached system of coordinates
$y_{0,c}$	critical value of particle's y coordinate at time $t = 0$

z^* z/d

Greek Letters

α ratio, defined in text

α_0, β_0, γ_0 integrals defined in text

β $b/a > 1$

Δ defined in text

ξ', η', ζ' fluid's vorticity coefficients,

ξ^0, η^0, ζ^0 location of droplet's center in the x', y', z' coordinate system

$\Delta\theta'$ angular separation in field of flow's grid.

θ angle between the z and z' coordinates (Fig. 2); $\dot{\theta} = d\theta/dt$

$\Delta\theta_B$ angle's change due to particle's Brownian motion

$\varphi(x',y',z')$ a function, defined in text

λ' a dummy variable

λ Lagrange's undetermined multiplier

χ_0 defined in text

μ medium's dynamic viscosity

ν kinematic viscosity of medium

ρ $(x^2 + y^2)^{1/2}$

ρ_1 density of the particle

σ_1, σ_2 statistical weights, defined in text

$\boldsymbol{\omega}$ rotational velocity of the particle; $\omega_{x'}$, $\omega_{y'}$, $\omega_{z'}$—components along rotating axes x', y', and z'

$\boldsymbol{\Omega}_R$ rotation tensor about center of fluid dynamic reaction R

ψ angle between line of nodes and the x' coordinate (Fig. 2); $\dot{\psi} = d\psi/dt$

ϕ angle between the x coordinate and the line of nodes (Fig. 2); $\dot{\phi} = d\phi/dt$

Φ probability density of a random particle's orientation

Subscripts

c denotes predetermined value of distance between particle's and droplet's surface

e stands for an external force or torque

F denotes fluid dynamic force or torque

i running index

M stands for a force, torque, or particle velocity taken with respect to center of mass; when succeeding u_M, it denotes value of undisturbed flow at the point occupied by particle's center of mass

R denotes a tensor taken with respect to center of fluid dynamic reaction

∞ stands for terminal state

1 denotes trajectory closest to the limiting one

0 stands for an initial state value

Other Symbols

$\square$ a vector operator, defined in text

ACKNOWLEDGMENT

This research was supported by a grant from the United States–Israel Binational Science Foundation (BSF), Jerusalem, Israel, whose help is gratefully acknowledged.

REFERENCES

1. Happel, J., and Brenner, H., "Low Reynolds Number Hydrodynamics," pp. 163–176, Prentice–Hall, Englewood Cliffs, N. J., 1965.
2. Brenner, H., *Chem. Eng. Sci.* **19**, 703–727 (1964).
3. Jeffery, G. B., *Proc. Roy. Soc.* **102A**, 161–179 (1923).
4. Fuchs, N. A., "The Mechanics of Aerosols," pp. 159–80. Pergamon, Oxford, 1964.
5. O'Donnel, H., Montgomery, T. L., and Corn, M., *Atmos. Environ.* **4**, 1–7 (1970).

6. Gallily, I., and Cohen, A.-H., *J. Colloid Interface Sci.* **56**, 443–459 (1976).
7. Gallily, I., and Eisner, A. D., *J. Colloid Interface Sci.* **68**, 320–337 (1979).
8. Walter, J. *et al.*, Experimental Determination of the Number and Size of Asbestos Fibers in Ambient Air, Final Report, Interagency Agreement (ARB3-688), Air and Industrial Hygiene Laboratory, Laboratory Service Branch, California Department of Health, 1976.
9. Gallily, I., and Mahrer, I., *Aerosol Sci.* **4**, 253–261 (1973).
10. Davis, M. H., *J. Geophys. Res.* **71**, 3101–3104 (1966).
11. Gans, R., *Ann. Phys. (Leipzig)* **86**, 628–656 (1928).
12. Cohen, A-H., and Gallily, I., *J. Atmos. Sci.* **34**, 827–842 (1977).
13. LeClair, B. P., Hamiliec, A. E., and Pruppacher, H. R., *J. Atmos. Sci.* **27**, 308–315 (1970).
14. Goldstein, H., "Classical Mechanics," p. 134. Addison-Wesley, Reading, Mass., 1950.
15. Smithsonian Meteorological Tables (R. J. List, Ed.), pp. 293, 395, 6 rev. ed. The Smithsonian Institution, Washington, D. C.
16. Gallily, I., "The Dynamics of Nonspherical Particles. III. Mobility and Deposition in Still Air," Final Technical Report, p. 19, European Research Office, U. S. Army, London NW1, England, Contract No. DAERO-75-G-002, 1977.
17. Fuchs, N. A., "The Mechanics of Aerosols," p. 245. Pergamon, Oxford, 1964.
18. Grover, S. N., Pruppacher, H. R., and Hamielec, H. H., *J. Atmos. Sci.* **34**, 1656–1663 (1977).